Nanoscale



PAPER View Article Online
View Journal | View Issue



Cite this: Nanoscale, 2019, 11, 2238

Direct conversion of carbon nanofibers and nanotubes into diamond nanofibers and the subsequent growth of large-sized diamonds

J. Narayan, 📵 *a A. Bhaumik, a R. Sachan, a,b A. Haque, a S. Gupta 📵 a and P. Panta

We report a pulsed laser annealing method to convert carbon fibers and nanotubes into diamond fibers at ambient temperature and pressure in air. The conversion of carbon nanofibers and nanotubes into diamond nanofibers involves melting in a super undercooled state using nanosecond laser pulses, and quenching rapidly to convert into phase-pure diamond. The conversion process occurs at ambient temperature and pressure, and can be carried out in air. The structure of diamond fibers has been confirmed by selected-area electron diffraction in transmission electron microscopy, electron-back-scatter-diffraction in high-resolution scanning electron microscopy, all showing characteristic diffraction lines for the diamond structure. The bonding characteristics were determined by Raman spectroscopy with a strong peak near 1332 cm⁻¹, and high-resolution electron-energy-loss spectroscopy in transmission electron microscopy with a characteristic peak at 292 eV for σ^* for sp³ bonding and the absence of π^* for sp² bonding. The Raman peak at 1332 cm⁻¹ downshifts to 1321 cm⁻¹ for diamond nanofibers due to the phonon confinement in nanodiamonds. These laser-treated carbon fibers with diamond seeds are used to grow larger diamond crystallites further by using standard hot-filament chemical vapor deposition (HFCVD). We compare these results with those obtained without laser treating the carbon fibers. The details of diamond conversion and HFCVD growth are presented in this paper.

Received 1st November 2018, Accepted 29th December 2018 DOI: 10.1039/c8nr08823c

rsc.li/nanoscale

1. Introduction

Direct conversion of carbon into diamond has fascinated scientists from all over the world for the longest time, because it is thermodynamically challenging with many exciting technological applications ranging from quantum computing, sensing and communication to field emission and tool coatings for oil and gas exploration and deep-sea drilling, in addition to diamond jewelry. 1,2 According to the thermodynamic equilibrium phase diagram, carbon/graphite can be converted into diamond at high temperature (5000 K) and pressure (12 GPa). These pressures and temperatures are somewhat reduced in the presence of catalysts. That is how diamond grits are produced industrially and nature accomplishes this naturally in the Earth's crust.³ For polycrystalline graphitic rods, lower temperatures (2573-2723 K) for diamond conversion at higher pressures (12-25 GPa) have been reported.4

Recently, we have reported a major breakthrough in the conversion of carbon thin films into diamond by overcoming thermodynamic constraints with the help of kinetics.^{5,6} By using high-power nanosecond laser pulses, amorphous carbon layers were melted in a highly undercooled state and quenched subsequently into phase-pure diamond or into a new phase of Q-carbon at a higher undercooling. Remarkably, parallel results were obtained for the conversion of h-BN into c-BN or Q-BN.⁷ These diamond and c-BN structures were doped with n- and p-type dopants with concentrations far higher than equilibrium thermodynamic solubility limits as a result of rapid quenching from the liquid and solute trapping phenomenon. We were able to control the nature and number density of defects in diamond and c-BN more precisely from the liquid phase growth, which is an important consideration for solidstate devices, as the annealing of the as-grown defects in these materials requires temperatures exceeding 1700 °C.⁷

These diamond structures can be used as seed precursors to grow large-sized diamond structures by hot-filament chemical vapor deposition (HFCVD) and microwave-plasma chemical vapor deposition (PECVD). The HFCVD and PECVD require seeding on which CH_x species are attached during diamond growth. Carbide forming substrates provide these nucleation sites. In the case of noncarbide forming substrates, strain

^aDepartment of Materials Science and Engineering, Centennial Campus, North Carolina State University, Raleigh, NC 27695-7907, USA. E-mail: narayan@ncsu.edu

^bMaterials Science Division, Army Research Office, Research Triangle Park, NC 27709, USA

temperatures.

Nanoscale

centers and surface roughening by scratching and pulsed laser annealing can provide some diamond nucleation sites. Onedimensional structures of diamond with sizes ranging from nano- to micrometers will play a crucial role in nanoscale devices with new functionalities, ranging from quantum computing, sensing and communication to efficient catalysts and field emission displays. The conversion of carbon tubes and fibers into diamond fibers/rods provides direct access to these devices. Diamond nanorods (DNRs) in the form of pillars have been created from polycrystalline8 and single-crystal diamond films⁹ by using microwave plasma and reactive ion etching methods. Other extensive research efforts in this area have focused on the direct formation of DNRs using CVD (chemical vapor deposition) methods and the direct conversion of carbon into diamond. This is a very expensive and cumbersome process with a limited yield of polycrystalline structures. The CVD based methods require atomic hydrogen and carbon containing species. The formation of DNRs with 4-8 nm diameter and ~100 nm length was reported by Sun et al. after prolonged (>20 h) hydrogen plasma treatment of carbon nanotubes at 1000 K. 10 Hsu et al. reported the synthesis of DNRs by chemical vapor deposition at ambient pressure by introducing hydrogen during the CNT growth process. 11 In both of these cases, nanotubes provide the source for the carbon containing

CH_x species and the nucleation sites for diamond growth.

These methods produce diamond mixed with amorphous

carbon with limited yield, and involve toxic gases at high

In the area of direct conversion, Wei et al. reported the conversion of carbon nanotubes into diamond through the formation of the carbon onion phase via solid-phase transformation. 12 The process involved coating of the carbon nanotubes on a cast iron substrate, followed by CO2 CW laser irradiation. Luo et al. reported the formation of diamond nanocrystals at the tips of carbon nanofibers after spark plasma sintering (SPS) at 1500 °C and atmospheric pressure, and explained it via the formation of an intermediate phase of carbon onion.¹³ Zhang et al. found the conversion of the tips of multi-walled carbon nanotubes (MCNTs) into diamond after SPS at 1200 °C and explained the conversion process by nanotube to carbon onion to diamond process.14 Ozden et al. showed that the ballistic fracturing of CNTs can lead to the formation of nanodiamonds, 15 which is consistent with the transformation of carbon nanotubes into diamond at high pressures and temperatures (4.5 GPa at 1300 °C). 16 More recently, J. Zhang et al. have shown the conversion of carbon nanotubes into T-carbon by using picosecond laser irradiation.¹⁷ Pérez del Pino et al.¹⁸ reported the formation of different forms of amorphous carbon, including nanodiamonds by using pulsed laser irradiation (266 nm NdYAG laser with 3 ns pulse duration and 40–100 mJ cm⁻²) of MWCNTs under a nitrogen atmosphere. However, characteristic Raman (near 1332 cm⁻¹) and EELS (at 292 eV) peaks for the diamond phase were not observed. The TEM fringe contrast, which is not very reliable, is reported for the [200] and [100] orientation. They meant the formation of (200) and (110) planes, which are not the diffracting planes of diamond.

Normally, the (111) planes should be present with cross-fringes for reliability based upon two sets of the {111} planes. It is envisaged that there is not enough undercooling due to very short laser pulses, which is the key to the formation of the diamond phase. It should be noted that none of these previous methods invoked melting and undercooling as the mechanism for the conversion of a carbon-based structure into diamond.

Here we report the conversion of carbon fibers (available inexpensively) and nanotubes into diamond fibers by nanosecond pulsed laser melting. In our previous work based on laser induced diamond conversion, we have shown that undercooling plays an important role. The sapphire, plastic, and glass substrates provide sufficient undercooling in the case of amorphous thin films of carbon. In the present case, the restriction of heat flow (1D) in CNT/CNF provides enough undercooling to cause the conversion. The melting in the middle of CNT/CNF leads to the formation of sp³ enriched amorphous carbon as a result of rapid heat flow and less undercooling. We have carried out detailed laser-solid interaction simulations to determine the optimized conditions for undercooling and conversion into diamond or a new phase of carbon, namely Q-carbon.⁵ The formation of beads at the tips of nanofibers and nanotubes provides direct evidence for the melting process. The conversion process starts at the tips and bends, which can be extended with the number of pulses to cover entire lengths. There is a critical diameter of the fiber below which there is a complete conversion into diamond. Above this critical size, diamond nanocrystallites are formed on the surface, some of which grow rapidly to form diamond nanorods normal to the substrate. These nanostructures are ideally suited for applications ranging from enhanced catalysis to field emission. We have used these laser-annealed fibers as seeds for further growth to obtain larger sizes and areas using conventional HFCVD (hot-filament chemical vapor deposition) and PECVD (plasma-enhanced chemical vapor deposition). We have compared these results from laser-annealed fibers with untreated carbon fibers, and found considerably enhanced diamond nucleation and growth in laser-annealed fibers.

2. Experimental

The CNFs are synthesized in a tube furnace-CVD chamber thermally baked at 800 °C. Highly sensitive mass flow controllers are used to introduce Ar (450 sccm) and H_2 (10 sccm) in the tube furnace prior to CVD processing. The temperature in the CVD furnace is ramped up to 800 °C and thermally soaked for 10 min. At this temperature, 25 sccm of C_2H_4 is introduced in the furnace for 30 minutes. After that, the Ar and H_2 gases are blown into the tube furnace and the flow of C_2H_4 is switched off. The temperature is then ramped down to room temperature for 2 hours. The prepared CNFs are ultrasonicated to remove unwanted metallic impurities. These CNFs are irradiated in air with ArF laser pulses (pulse duration = 20 ns, wavelength = 193 nm, energy density = 0.6–1.0 J cm $^{-2}$). Due to

Paper Nanoscale

the restriction of heat flow in one-dimensional CNFs, melting of amorphous carbon occurs, leading to a highly undercooled state. The undercooled state is subsequently quenched to form nanostructures of diamond. On increasing the number of nanosecond laser pulses, the entire fibers are converted into diamond fibers (DNFs). The CNFs (before and after PLA processing) are dispersed in ethanol and transferred onto copper TEM grids. To facilitate the bleeding of electronic charges, the sample is sandwiched between two copper grids and then mounted in the TEM sample holder. The laser-annealed carbon fibers were used for seeding the diamond growth by HFCVD (hot-filament chemical vapor deposition with 2.0% CH₄ in H₂) at a substrate temperature of 1100 K and a filament temperature of 2300 K. These structures are characterized by TEM, SAED, EBSD, SEM, and Raman spectroscopy (using 532 nm excitation laser). High-resolution SEM (and EDX) and EBSD (electron-scatter-back diffraction) measurements are carried out using FEI Verios 460L SEM and FEI Quanta 3D FEG FIB-SEM, respectively. The EBSD technique provides three-dimensional (Kikuchi) diffraction patterns for phase identification and the structural morphology is determined by high-resolution SEM. A JEOL 2000 FX and FEI Titan 80-300 microscopes are used for performing the TEM, EELS and SAED of the CNFs and DNFs. A 200 kV electron beam from a LaB6 source (having point-to-point resolution of 0.14 nm) is used for the TEM imaging and diffraction. A HORIBA Xplora PLUS confocal Raman microscope having 0.5 µm spatial resolution and 532 nm excitation source is used for determining the Raman active vibrational characteristics (at 300 K) of the CNFs and DNFs. Raman spectroscopy provides a distinctive identification of diamond and related materials.

3. Results and discussion

Fig. 1 shows a SEM micrograph of pristine carbon nanofibers before pulsed laser annealing where the structure of carbon is

(a) Before PLA (b) After PLA

50 nm

50 nm

Fig. 1 High-resolution SEM images of (a) a CNF before PLA and (b) a CNF after PLA showing the conversion of carbon nanofibers into diamond nanofibers.

amorphous and contains some surface roughness (Fig. 1a). This surface roughness increases with the size or the diameter of the nanofiber. After a single 20 ns (193 nm ArF) laser pulse at ambient temperature and pressure, we observed a direct conversion of carbon nanofiber into crystalline diamond (Fig. 1b). The conversion process starts at the tips and bends and is more efficient for thinner fibers (less than 50 nm diameter). Fig. 1(b) shows a comparison of the conversion of a thin 35 nm diameter fiber, whereas a 60 nm diameter fiber shows the formation of nanodiamonds only on the surface. The fiber orientation also plays an important role with more efficient conversion for fibers aligned along the beam. Fig. 2 shows a large number of carbon fibers after laser annealing with 10 laser pulses, where the effect of the size (diameter) and the orientation of fibers with respect to the laser beam is clearly shown. The carbon fibers with diameters less than 50 nm are converted fully into diamond, whereas larger diameter fibers show the formation of diamond on the surface. These diamond nuclei on the surface can grow normal to the carbon fiber during irradiation with subsequent pulses. From the length of the diamond fiber, the diamond growth velocities are estimated to be about 2 ms⁻¹, which is consistent with the theoretical modeling presented below. These nanostructures are ideally suited for diamond-based catalytic applications.

The crystal structure determination of the as-grown DNFs was carried out by the electron beam scatter diffraction (EBSD) technique in a high-resolution SEM, as shown in Fig. 3. The EBSD is a powerful non-destructive technique to determine the details of the atomic structure of crystalline phases by providing three-dimensional diffraction (Kikuchi) patterns. The electron probe size used for EBSD is ~ 10 nm, and thus it is ideal for the determination of the structure along the length of the diamond fiber. The EBSD results are shown in the inset in Fig. 3 from the encircled region near the tip of the fiber. The characteristic Kikuchi diffraction pattern of diamond and relative orientation are depicted in a red cube. There was minimal

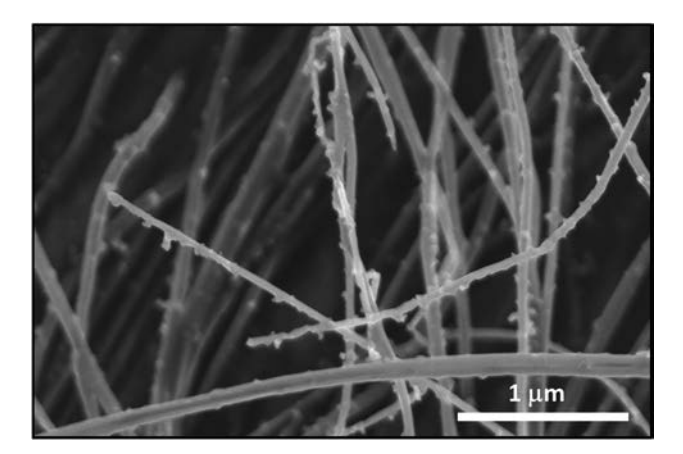


Fig. 2 High-resolution SEM image showing the conversion of carbon nanofibers of different diameters, where thin fibers are completely converted into diamond and thick fibers show diamond formation on the surface. Some of the surface nuclei grow into nanodiamond rods normal to the substrate along the diameter.

Nanoscale Paper

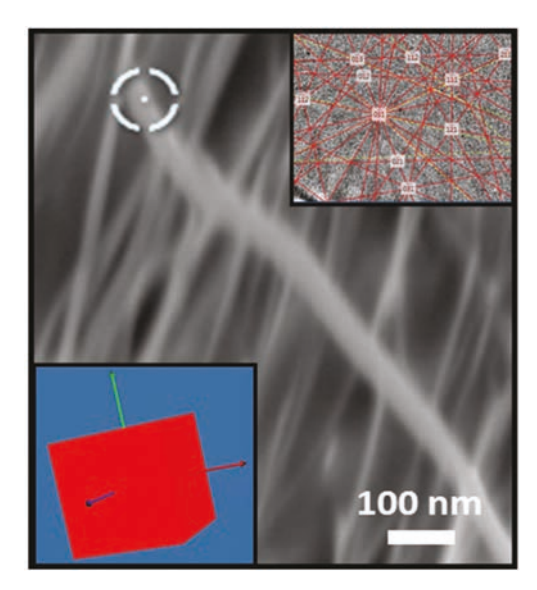


Fig. 3 SEM micrograph of laser treated fibers with the EBSD (Kikuchi) pattern characteristic of diamond and relative orientation (red cube) of the diamond formed.

change in the crystal orientation (Kikuchi diffraction pattern) along the length from the tip, as revealed by the EBSD patterns. The highest undercooling occurs at the tip and decreases as we move more towards the base (of CNF). The amorphous nature of the CNF was found to be unaltered close to its base. Fig. 4(a) shows the Raman results from carbon nanofibers before and after laser treatment. The Raman peak corresponding to nanodiamonds is observed at \sim 1321 cm⁻¹ in the CNF samples after PLA processing. Fig. 4(b) shows the

Raman spectra of the CNT after PLA. The peak at 1324.2 cm⁻¹ corresponds to the diamond formed after PLA. The downshift (from 1332 cm⁻¹ in microdiamonds) and spectral broadening are due to phonon confinement19 in nanosized diamonds (formed after PLA). Therefore, Raman studies provide clear and consistent evidence for conversion of CNFs into nanodiamonds (due to laser-assisted melting and resolidification) after PLA treatment. Fig. 5 depicts the TEM (transmission electron microscopy) and SAED (selected-area electron diffraction) analyses of carbon fibers after laser annealing. Fig. 5(a) shows the formation of diamond near the tip of the carbon fibers. The SAED pattern covering many nanodiamond tips, which are oriented differently, is shown in Fig. 5(b). The SAED pattern shows a characteristic diffraction pattern (diffraction rings) of nanocrystalline diamond with the distinct diffraction peaks of the 111, 200, 220, 311, 222, 004, 331, and 333 planes. We observe the (200) diffraction ring in TEM due to multiple diffractions from two sets of the (111) and (1-1-1) planes. The diffraction from the base of the fiber contained a characteristic amorphous structure, which is similar to that of unirradiated carbon. Fig. 5(c) depicts the SEM-EDX of the tip of the DNF (formed after PLA). The EDX spectrum depicts the presence of only the C-Kα₁ peak at 0.277 keV (and no other impurity peaks). This shows that the phase transformation of the amorphous CNF into diamond occurs in the absence of a catalyst (at room temperatures and atmospheric pressures). Highresolution electron-energy-loss spectroscopy in transmission electron microscopy showed a characteristic peak at 292 eV for σ^* for sp³ bonding and the absence of π^* at 284 eV for sp² bonding.

Fig. 6(a) shows the theoretical calculation of the melt depth as a function of time of the carbon substrate. Carbon is found

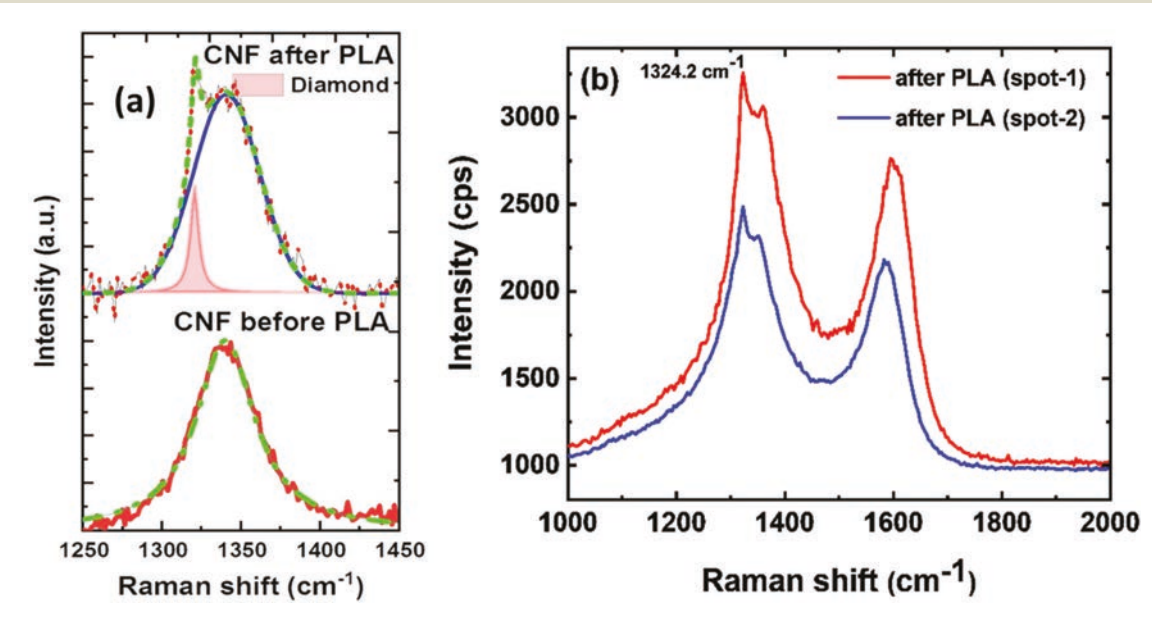


Fig. 4 (a) Raman spectra before and after laser annealing in a CNF, clearly showing the diamond peak near 1321 cm⁻¹, which downshifted from the standard 1332 cm⁻¹ peak as a result of phonon confinement, and (b) Raman spectra after PLA in a CNT showing the sharp diamond peak at 1324.2 cm⁻¹.

Paper Nanoscale

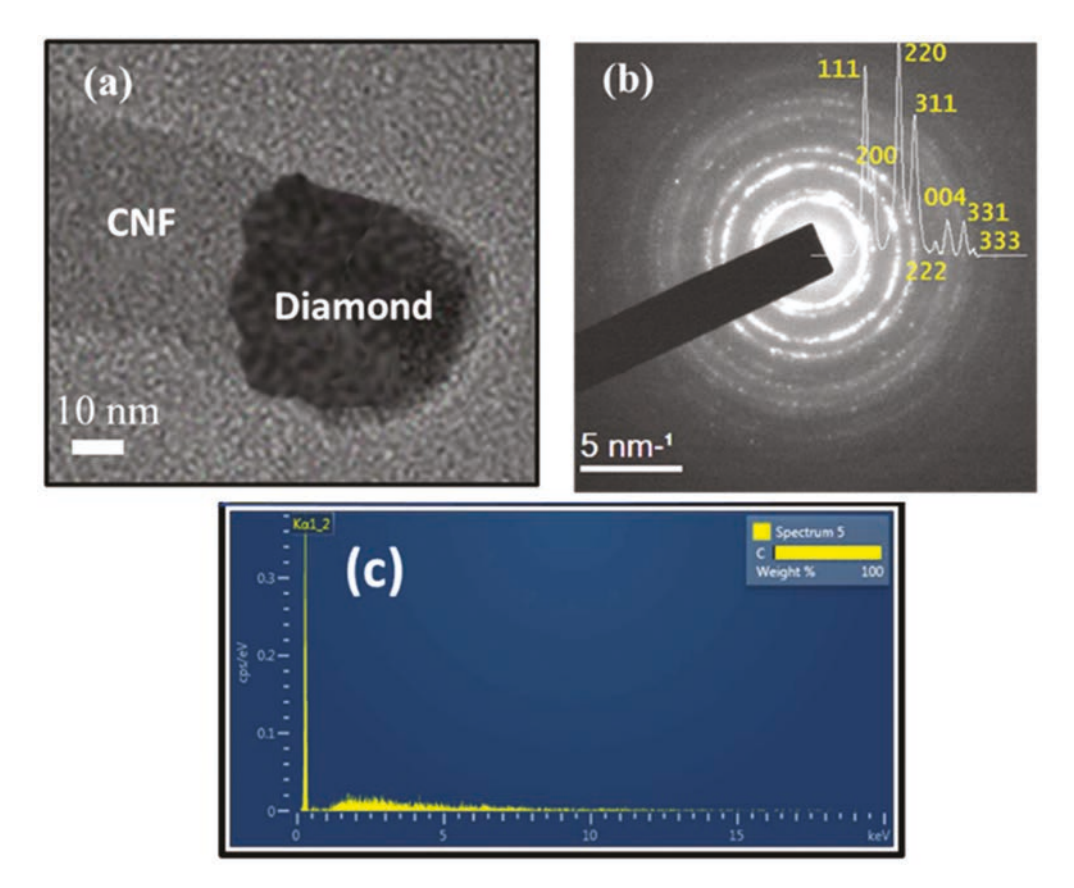


Fig. 5 (a) TEM micrograph showing a carbon nanofiber and diamond formation at the tip, (b) SAED pattern showing the characteristic diamond diffraction rings, and (c) SEM-EDX of a CNF after PLA.

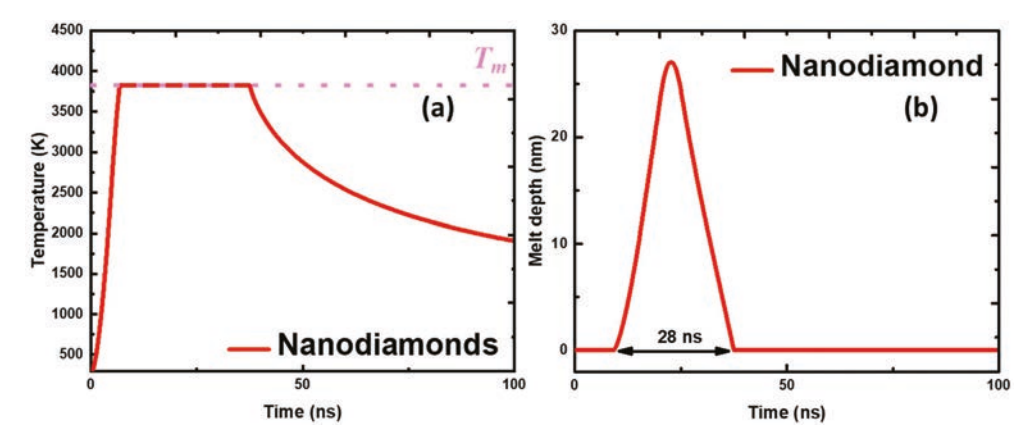


Fig. 6 SLIM calculations using the following parameters: melting temperature: 3823 K, evaporation temperature: 5000 K, latent heat of melting: $19\,775\,\mathrm{J}\,\mathrm{cm}^{-3}$, thermal conductivity of solid: $3\,\mathrm{W}\,\mathrm{m}^{-1}\,\mathrm{K}^{-1}$, thermal conductivity of molten carbon: $2.9\,\mathrm{W}\,\mathrm{cm}^{-1}\,\mathrm{K}^{-1}$, absorption coefficient in the solid state: $8.00\,\mathrm{x}\,10^{5}$, absorption coefficient in the liquid state: $1.00\,\mathrm{x}\,10^{6}$, reflectivity in the solid state: 0.3, reflectivity in the liquid state: 0.6, annealing energy density: $0.6\,\mathrm{J}\,\mathrm{cm}^{-2}$, laser pulse width: $20\,\mathrm{ns}$.

to melt in a highly undercooled state, and quenching from this state leads to the formation of diamond. The melting starts after 10 ns of the incidence of the laser pulse, and the melt-in front rapidly penetrates until the end of the laser pulse. After that solidification occurs with the underlying seed. As shown in the figure, the solidification velocity is of the order of 2–5 ms $^{-1}$. The temperature profile in Fig. 6(b) shows that amorphous carbon melts at $\sim\!4000$ K in a highly undercooled state, close to 1000 K below the equilibrium melting of graphite. The pulsed laser annealing process is carried out under atmospheric pressure and room temperature (in air). No external heat is applied during the conversion. The tempera-

Nanoscale

ture of ~4000 K is attained after the laser-material interaction, and this undercooled state results in the formation of diamond upon quenching. During the transformation of CNTs and CNFs, the temperature rises locally to 4000 K, but it is for a very short time, often less than 100 ns. As a result, the overall temperature rise of the system is less than 5 K. These calculations were performed using the SLIM computer program using the heat flow equations under the finite-element modeling scheme.20 The pulsed laser annealing of nanofibers leads to melting of carbon, and subsequent quenching from a highly undercooled state results in the direct conversion of carbon into diamond. Our earlier studies on melting of amorphous carbon films on sapphire substrates have shown that molten carbon can be converted into diamond at an undercooling at ~1000 K, and into a new form of carbon (named Q-carbon) at a higher undercooling at ambient temperatures and pressures in air.

Fig. 7 shows the conversion of carbon nanotubes into diamond nanofibers after 10 laser shots at 0.65 J cm⁻² of an ArF laser. The conversion process in the case of nanotubes is

similar to that of nanofibers, as the conversion process starts from the tips and bends, and it is more efficient for both nanotubes and fibers which are aligned normal to the substrate. The diameter of the carbon nanotubes ranged from 10 to 50 nm (mostly double-walled) with over 300 nm in length. Fig. 7(a) shows a low-magnification SEM image, showing nanotubes of varying sizes with diamond formation near the tips. The diamond tips are considerably sharper due to the smaller amount of carbon available in the hollow nanotubes. The details of diamond conversion near the tips are shown in Fig. 7(b) and (c), where nanodiamond beads are formed with direct evidence of carbon melting during the conversion process. Fig. 7(d) shows the formation of nanodiamonds normal to the carbon nanotubes (marked with arrows). These results show the formation of the sharpest diamond nanoneedles by the direct conversion of carbon nanotubes into diamond.

A detailed electron microscopic analysis is performed on the laser annealed CNTs, and the results are shown in Fig. 8. A

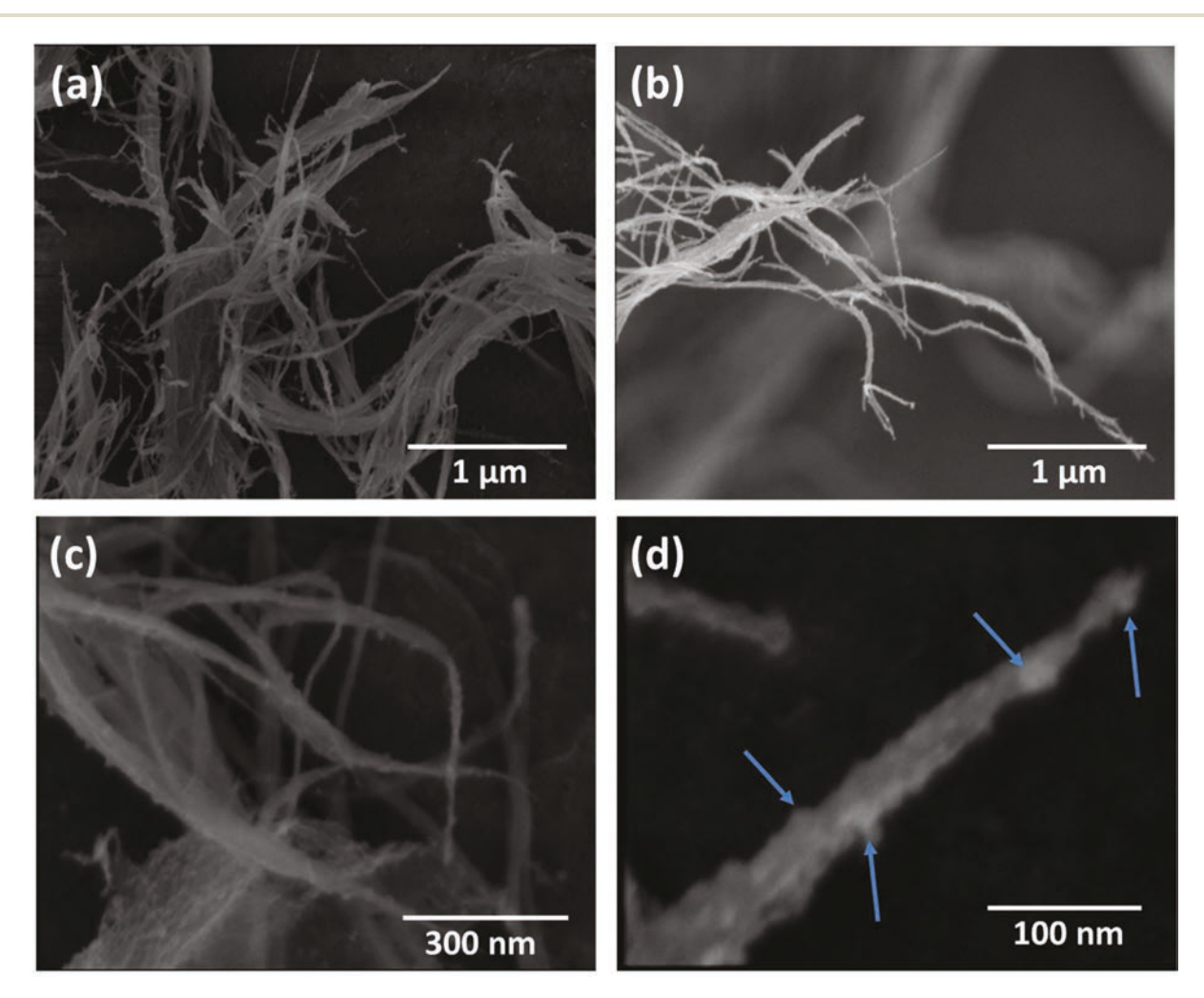


Fig. 7 Conversion of carbon nanotubes into diamond nanorods; (a) SEM micrograph showing conversion of carbon nanotubes into diamond after 10 pulses of an ArF laser (pulse duration 20 ns) at 0.65 J cm⁻²; (b) and (c) details of the conversion process starting from the tips; and (d) nucleation of diamond in the middle of the nanotube and growth of diamond nanorods normal to the tube (shown by arrows).

Paper

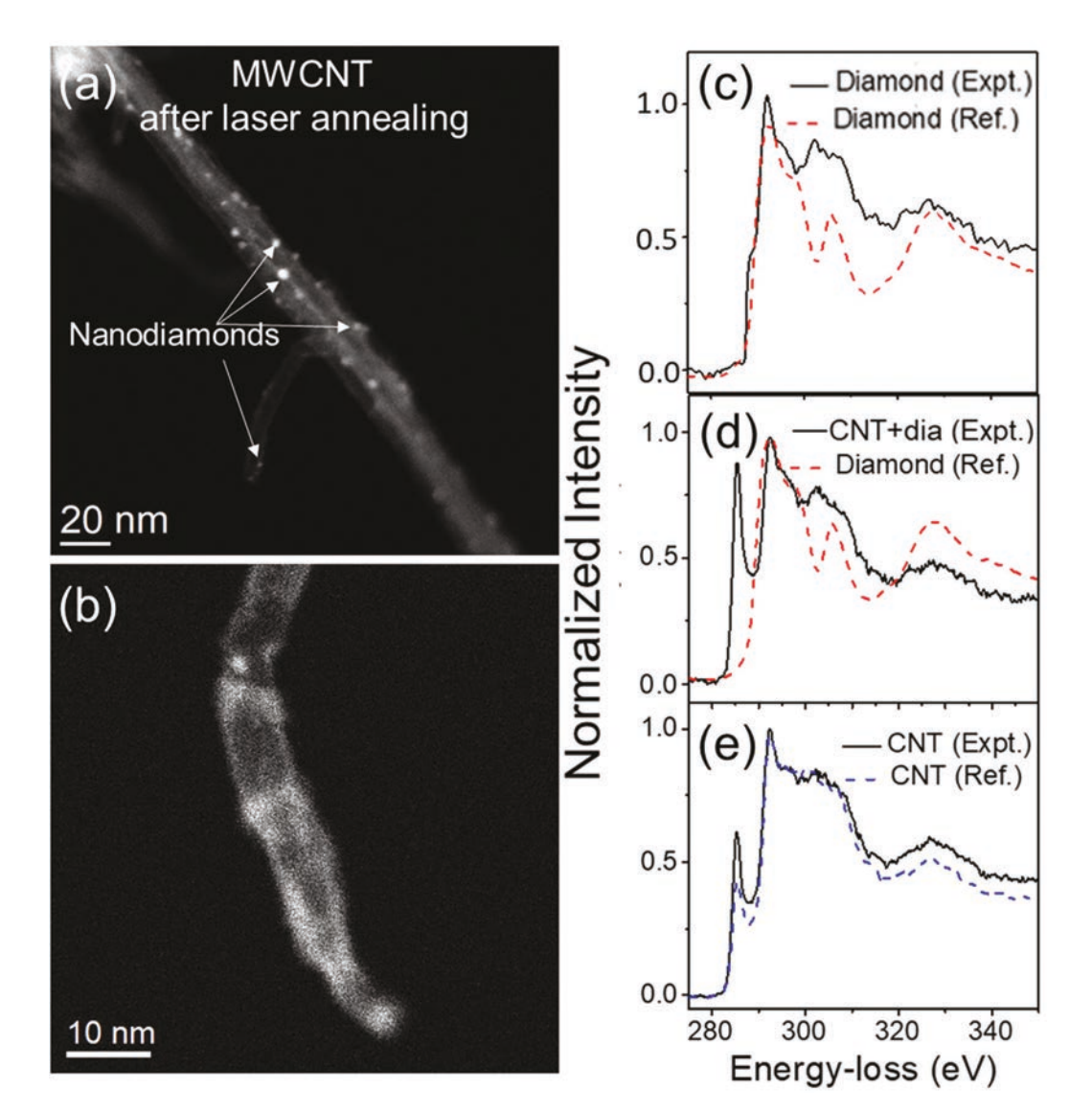


Fig. 8 (a) HAADF image of CNTs after laser annealing showing the formation of nanodiamonds, (b) HAADF image of a single CNT showing the formation of nanodiamonds at its edges and the end, EELS spectra of the (c) diamond, (d) CNT and diamond obtained from the corresponding regions in a laser annealed CNT, and (e) CNT before pulsed laser annealing. The reference spectra of the diamond and CNT are also shown in (c) and (e), respectively for comparison.

representative HAADF image of laser annealed CNTs is presented in Fig. 8a, demonstrating the formation of nanodiamonds in various regions on CNTs. The average size of the nanodiamonds is estimated to be \sim 3 \pm 1 nm, while CNTs are found to be \sim 7 \pm 1 nm in diameter. Fig. 8b further shows the formation of nanodiamonds on an individual CNT, clearly showing the emergence of nanodiamonds at the tip of the CNT. This supports the previously proposed hypothesis of diamond formation through ultrafast melting and non-equilibrium super undercooling of CNTs. Various diamonds are also observed on the body of CNTs formed under similar conditions but through partial melting of CNTs. We have also performed EELS at ~700 eV where no peaks of Fe are observed. SEM-EDX also shows no Fe content in the CNFs/CNTs. In addition, the contrast in the ADF image is primarily arising

due to the thickness and density of the material, as the density of diamond is ~3 times higher than that of CNTs. Using lowloss EELS, the relative thickness (long ratio) of diamond is estimated to be 0.80, while that in the neighboring CNT region is 0.15. The electron energy-loss (EEL) spectra obtained from the nanodiamonds, CNT and nanodiamonds, and unannealed CNT are shown in Fig. 8(c), (d) and (e), respectively. The spectra are shown along with the reference CNT and diamond EEL spectra for comparison. The EEL spectrum obtained from the nanodiamonds (Fig. 8(c)) exhibit the near edge fine structure peaks at 292, 297, 305, and 326 eV, which are broader than the typical reference spectrum from diamonds. The broadening in the characteristic peaks is attributed to the strained nature of nanodiamonds. The EELS in Fig. 8(c) is acquired from the region in the converted nanodiamond

Nanoscale

where the π^* peak is clearly absent. As shown in Fig. 8(d), the EEL spectrum suggests diamond and CNT regions to be overlapping which is found very frequently during the analysis. The additional strong π^* (284 eV) peak is clearly observed in Fig. 8(d). The appearance of the π^* peak is due to the presence of the underlying CNT. The EEL spectrum obtained from the CNT appears to be consistent with the typical reference spectra. It should be mentioned that under intense electron flux due to the small probe-size during EELS, diamond was found to convert into nanodiamonds and amorphous graphitic phase of carbon.

Fig. 9(a) shows the formation of large diamond crystallites in the HFCVD reactor after deposition for three hours by using the seeding of laser annealed diamond nanofibers. These crystallites have remarkably uniform size, where the average size of the diamond crystallites was determined to be 2.2 µm. This is consistent with average diamond nuclei of about 100 nm with a growth rate of about 700 nm h⁻¹. The 100 nm diamond nuclei are formed from undercooled liquid carbon in 50 ns with a diamond growth rate of about 2 ms⁻¹. Fig. 9(b) shows diamond HFCVD growth on carbon nanofibers which were not treated with lasers. The number density of diamond crystallites is considerably higher for laser-annealed fibers (Fig. 9(a)) compared to that of untreated carbon fibers (Fig. 9(b)). The laser treated fibers are totally consumed by diamond growth, because of the much higher number density of diamond nuclei formed after laser annealing. In the case of untreated fibers, the number density of diamond nuclei is considerably lower, as they are formed on the surface of the fibers associated with strain centers and pits. The laser-treated fibers are totally consumed with a very high number density of diamond crystallites, as shown in Fig. 10(a) at a higher magnification. Fig. 10(b) shows the growth of diamond crystallites on the surface of untreated carbon fibers. These diamond crystallites merge and lead to the formation of larger size crystallites. Both treated and untreated fibers show secondary nucleation of diamond crystallites. It should be mentioned that the source for carbon in diamond growth is enhanced due to the additional carbon containing species from the fibers. In the treated samples, nanodiamond nuclei formed after laser annealing provide very effective nucleation sites. In the untreated samples, diamond nucleation starts from the surface roughness at pits, which may provide strain centers for diamond nucleation and subsequent growth. It should be mentioned that there is hardly any diamond growth observed

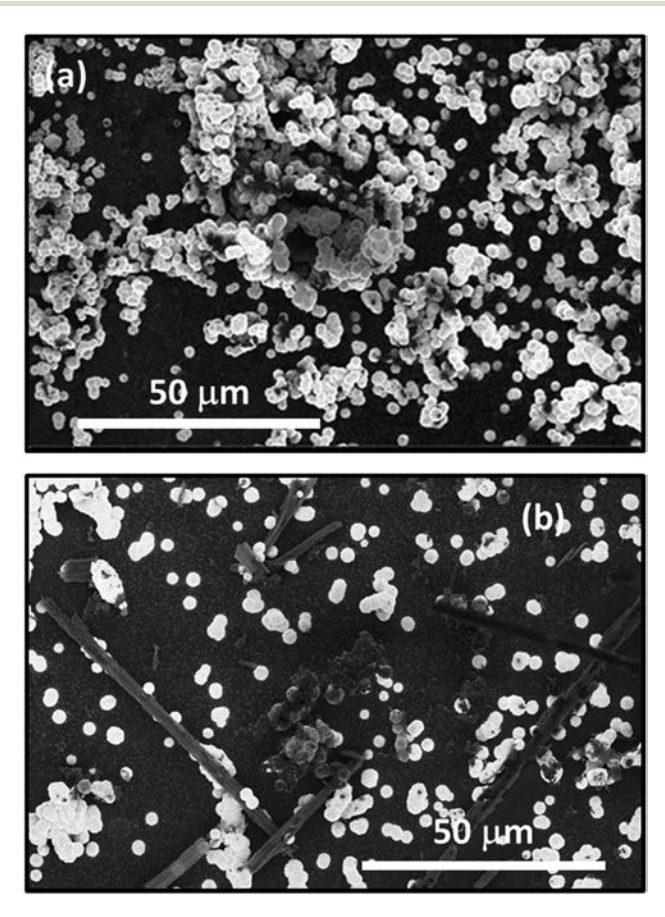
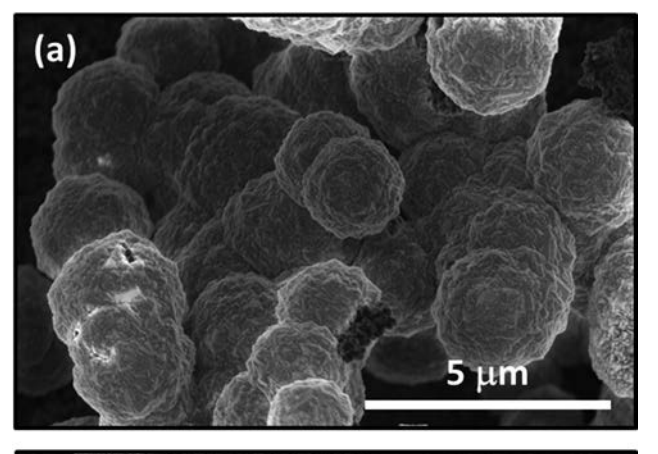


Fig. 9 (a) HFCVD growth of diamond after laser annealing of carbon fibers (five micron diameter) with one pulse and (b) HFCVD growth on untreated carbon fibers for comparison.



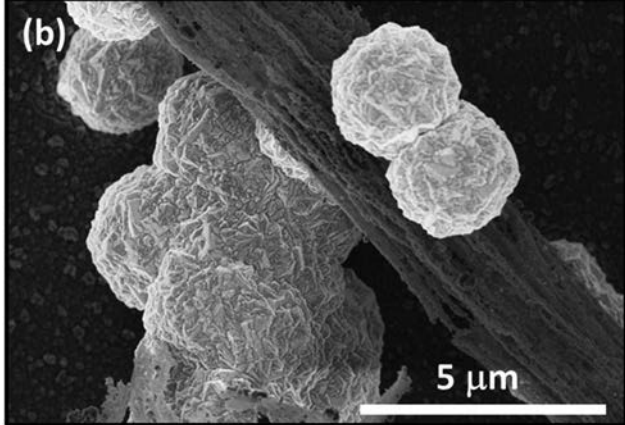


Fig. 10 (a) Mechanism of HFCVD growth from laser treated fibers, showing multiple layers of diamond growth and (b) details of HFCVD growth of diamond on untreated fibers. Laser treated fibers provide much more effective sites for diamond growth during HFCVD.

Paper Nanoscale

on pristine sapphire three-hour HFCVD growths. Fig. 11 shows characteristic Raman spectra results from diamond after HFCVD growth from laser treated and untreated samples. The Raman peak at 1331.26 cm⁻¹ is only slightly down-shifted from the bulk diamond peak at 1332 cm⁻¹, indicating the presence of nanocrystalline diamond. The presence of a G-peak at 1580 cm⁻¹ (associated with graphitic carbon) is very weak for diamond growth in laser treated fibers, characteristic of high-quality phase pure diamond. The G peak is more pronounced in untreated samples (CF-CVD-4F) due to the presence of unconsumed carbon fibers, compared to laser-treated samples (CF-CVD-1S-4F).

The formation of DNFs starts with the nucleation of diamond from the highly undercooled state of molten carbon (formed after PLA). The formation of diamonds occurs by homogeneous nucleation from the highly undercooled state of carbon. The change in Gibbs free energy (ΔG_T) associated with the formation of DNFs consists of a gain in volume energy $(\sim r^3)$ at the expense of surface energy $(\sim r^2)$, where r is the radius of the diamond nucleus. The change in free calculated using energy can be equation: $\Delta G_T = rac{-4}{3}\pi r^3rac{
ho}{M_{
m m}}rac{\Delta H_{
m m}}{T_{
m m}}\Delta T_{
m u} + 4\pi r^2 r_{
m s},$ where ho is the density of diamond, $\Delta H_{\rm m}$ is the latent heat of melting, $M_{\rm m}$ is the molar mass, and r_s is the surface free energy between diamond nuclei and the undercooled state of carbon. The first term in the equation is the volume energy term (gain in free energy for the formation of diamond nucleus from the undercooled state), whereas the second one is the surface energy term. The degree of undercooling, $\Delta T_{\rm u}$, is equal to $T_{\rm m}-T_{\rm r}$, where $T_{\rm m}$ indicates the melting point of graphite (\sim 5000 K) and T_r indicates the nucleation temperature (~4000 K). With an increase in the value of $\Delta T_{\rm u}$, $\Delta G_{\rm T}$ becomes more negative and a conversion of graphite (CNFs) into diamond (DNRs) is favorable.

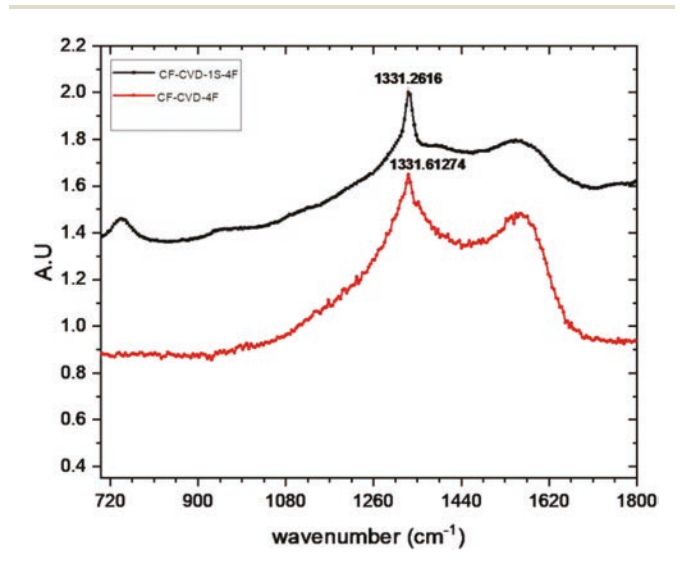


Fig. 11 Characteristic Raman spectra from HFCVD grown diamond on treated and untreated carbon fibers, showing some graphitic peaks in untreated samples.

Again, the critical radius and the change in Gibbs free energy (at $\frac{d\Delta G_{\rm T}}{dr} = 0$) are inversely proportional to $\Delta T_{\rm u}$ and $\Delta T_{\rm u}^2$, respectively. Therefore increasing $\Delta T_{\rm u}$ reduces the critical value of the diamond's radius and the change in Gibbs free energy (ΔG_T^*) . The rate of nucleation (I) is given by the equation: $I \sim \exp{\frac{-\Delta G_{\mathrm{T}}^*}{KT_{\mathrm{r}}}}$. Therefore, with a decrease in the value of ΔG_{T}^* , the rate of nucleation increases thereby facilitating the formation of diamond. For a 10 nm size nanodiamond, the estimated growth time is about 5-10 ns. This time requirement emphasizes the importance of the thermal conductivity of the substrate during rapid pulse laser heating. A rough estimate of r^* for diamond nuclei from the equation is ~20 Å, where the diamond surface free energy r_s is 0.6 J m⁻², T_m = 4000 K, $\Delta H_{\rm m}$ = 1.0 eV per atom, $\Delta T_{\rm u}$ = 1000 K, and ρ = 3.5 g cm⁻³. This is verified experimentally in our earlier papers on diamond^{5,6} and on silicon.²¹⁻²³ The growth velocity (ν) is directly related to the undercooling through the following equation: $v = \frac{D_{\infty}f}{\lambda f_{\rm D}} \left(1 - e^{\frac{(T_{\rm m} - T_{\rm u})\Delta S}{kT}}\right)$, where D_{∞} , f, λ , $f_{\rm D}$, k, T, $T_{\rm m}$, $T_{\rm u}$ and ΔS denote the liquid diffusivity ($\sim 10^{-8} \text{ m}^2 \text{ s}^{-1}$ in the liquid state), fraction of the available sites, atomic jump distance, geometrical factor associated with diffusion, Boltzmann constant, temperature, melting temperature, undercooling temperature, and the change in entropy, respectively. An increase in the value of T_{ij} decreases the value of the chemical free energy barrier for graphite to crystalline diamond phase transformation. This also increases the velocity of the meltfront. Therefore, the values of undercooling dictate the conversion of the amorphous graphitic phase into diamond via the carbon melt. If the cooling rate is slow (low undercooling and low solidification velocity), crystalline graphite is formed, whereas with high cooling rates (large undercooling and large solidification velocity), crystalline diamond is formed. We have synthesized diamond nanofibers from carbon nanofibers and carbon nanotubes by using a highly non-equilibrium technique of pulsed laser annealing. We have incorporated carbon nanofibers and carbon nanotubes on metallic substrates and irradiated with lasers to create highly efficient field emission devices. Upon irradiating the CNFs with the nanosecond ArF laser, the tips and bends of the CNFs are melted in a highly undercooled state. The highly undercooled state of carbon is a metastable phase and nanodiamonds nucleate from this state. The process (rapid melting, solidification, and growth) is completed in less than 200 ns. Our results clearly indicate that diamond can be formed under ambient conditions in air from the super undercooled state of molten carbon without a catalyst and atomic hydrogen (CVD process). The nanosecond laser parameters and heat confinement by the one-dimensional CNFs determine the temperature distribution and undercooling and play a critical role in the nucleation and growth of nanodiamonds. The nanosecond laser pulses help us achieve the undercooled state of carbon, and upon subsequent quenching, lead to the formation of nanodiamonds from

CNFs. The nanosecond laser heating and temperature distri-

butions are confined spatially and temporally. Therefore, the tips (and bends) of CNFs melt whereas the underlying areas are unaffected. By subsequent laser pulses, these diamond regions can be extended to form larger diamond nanofibers and nanorods. The key consideration is undercooling, which depends upon thermal properties and heat flow geometry. By simulating the heat flow²⁰ and taking into account the thermal properties for specific shapes, we can obtain the laser parameters needed for the conversion into diamond. These nanorods and nanofibers can be doped with N and Si to create N-V and Si-V centers for quantum communication, quantum sensing and quantum computing. These nanostructures can be doped with both n-type (such as N and P) and p-type (such as B) dopants for novel solid-state devices and high-efficiency field emitters. The formation of DNFs and their heterostructures will also have exciting applications ranging from drug delivery to optoelectronics and cellular sensors. 24 By controlling the nucleation and growth processes from the liquid, we can control the formation of defects and create diamond structures with fewer undesirable defects. This is a very important consideration in diamond as the defect annealing temperatures exceed 1700 °C, above which high pressure is needed to stabilize the diamond and anneal out defects. Such high temperatures and pressures needed for annealing defects in diamond do not render CVD grown diamonds very useful for the fabrication of solid-state devices.²⁵

4. Summary

In our method, carbon nanotubes and carbon fibers are melted in a super undercooled state using high-power nanosecond laser pulses, and quenched rapidly to convert them into phase-pure diamond rods. The conversion process occurs at ambient temperature and pressure, and can be carried out in air. This process of conversion of carbon into diamond can be scaled up by laser scanning, where a 200 Hz laser can generate 200 cm² area per second. Our method leads to the formation of phase-pure diamond rods across the scale ranging from a few nanometers to micrometers and beyond, depending upon the initial size of carbon nanotubes and carbon fibers. The diamond-tipped carbon nanofibers and carbon nanotubes grown on metallic substrates provide ideal field emitters for the next-generation contact-less energy-transfer systems and motors. This process can be scaled up to cover a large area over 100 to 200 cm² per second using 100 to 200 Hz (repetition rate per second). These nanofibers can be doped selectively with n- and p-type dopants with concentrations far higher than thermodynamic solubility limits, by incorporating dopants before melting for a variety of potential applications ranging from quantum sensors to efficient catalysts and field emitters. The nano- and microdiamonds have been used very effectively as seeds to grow large diamonds by CVD methods for a variety of applications ranging from abrasive powders for oil and gas exploration to diamond jewelry. This discovery of the conversion of CNF tips into diamond nanofibers at room

temperature and atmospheric pressure will open a new frontier for the synthesis and processing of diamond nanostructures for a variety of applications ranging from quantum computing, sensing and communication to field emission and tool coatings for oil and gas exploration and deep-sea drilling, in addition to diamond jewelry.

Conflicts of interest

There are no conflicts to declare.

Acknowledgements

We are grateful to the Fan Family Foundation Distinguished Chair Endowment for Professor J. Narayan, and this research was funded by the National Science Foundation (DMR 1735695). We are also very pleased to acknowledge the technical help from and useful discussions with Professors Yuntian Zhu, John Prater and Roger Narayan.

References

- 1 J. C. Angus and C. C. Hayman, Science, 1988, 241, 913-921.
- 2 J. Narayan, V. P. Godbole and C. W. White, *Science*, 1991, 252, 416–418.
- 3 F. P. Bundy, H. T. Hall, H. M. Strong and R. H. Wentorf, Nature, 1955, 176, 51–55.
- 4 T. Irifune, A. Kurio, S. Sakamoto, T. Inoue and H. Sumiya, *Nature*, 2003, 421, 599–600.
- 5 J. Narayan and A. Bhaumik, J. Appl. Phys., 2015, 118, 215303.
- 6 J. Narayan and A. Bhaumik, APL Mater., 2015, 3, 100702.
- 7 J. Narayan and A. Bhaumik, APL Mater., 2016, 4, 20701.
- 8 M. Pelliccione, A. Jenkins, P. Ovartchaiyapong, C. Reetz, E. Emmanouilidou, N. Ni and A. C. Bleszynski Jayich, *Nat. Nanotechnol.*, 2016, **11**, 700–705.
- 9 Y. Ando, Y. Nishibayashi and A. Sawabe, *Diamond Relat. Mater.*, 2004, 13, 633–637.
- 10 L. T. Sun, J. L. Gong, D. Z. Zhu, Z. Y. Zhu and S. X. He, Adv. Mater., 2004, 16, 1849–1853.
- 11 C.-H. Hsu, S. G. Cloutier, S. Palefsky and J. Xu, *Nano Lett.*, 2010, **10**, 3272–3276.
- 12 B. Wei, J. Zhang, J. Liang and D. Wu, *Carbon*, 1998, **36**, 997–1001.
- 13 C. Luo, X. Qi, C. Pan and W. Yang, Sci. Rep., 2015, 5, 13879.
- 14 F. Zhang, J. Shen, J. Sun, Y. Q. Zhu, G. Wang and G. McCartney, *Carbon*, 2005, 43, 1254–1258.
- 15 S. Ozden, L. D. Machado, C. Tiwary, P. A. S. Autreto, R. Vajtai, E. V. Barrera, D. S. Galvao and P. M. Ajayan, ACS Appl. Mater. Interfaces, 2016, 8, 24819–24825.
- 16 W. K. Wang and L. M. Cao, Russ. Phys. J., 2001, 44, 178– 182

Paper

17 J. Zhang, R. Wang, X. Zhu, A. Pan, C. Han, X. Li, D. Dan

- Zhao, C. Ma, W. Wang, H. Su and C. Niu, Nat. Commun., 2017, 8, 683.
- 18 Á. Pérez del Pino, E. György, L. Cabana, B. Ballesteros and G. Tobias, J. Appl. Phys., 2014, 115, 93501.
- 19 S. Prawer and R. J. Nemanich, Philos. Trans. R. Soc., A, 2004, 362, 2537.
- 20 R. K. Singh and J. Narayan, Mater. Sci. Eng., B, 1989, 3, 217-230.
- 21 J. Narayan and C. W. White, Appl. Phys. Lett., 1984, 44, 35-37.
- 22 J. Narayan, C. W. White, O. W. Holland and M. J. Aziz, J. Appl. Phys., 1984, 56, 1821.
- 23 R. F. Wood, D. H. Lowndes and J. Narayan, Appl. Phys. Lett., 1984, 44, 770.
- 24 R. Narayan, Diamond-based materials for biomedical applications, Woodhead Publishing, 2013.
- 25 A. M. Zaitsev, Proc. Natl. Acad. Sci. U. S. A., 2008, 105, 17591-17592.